JOURNAL OF AGRICULTURAL AND FOOD CHEMISTRY

Article

pubs.acs.org/JAFC

Solid-State Selective ^{13}C Excitation and Spin Diffusion NMR To Resolve Spatial Dimensions in Plant Cell Walls

Marcus Foston,[†] Rui Katahira,[‡] Erica Gjersing,[‡] Mark F. Davis,[‡] and Arthur J. Ragauskas*[,†]

[†]BioEnergy Science Center, School of Chemistry and Biochemistry, Institute of Paper Science and Technology, Georgia Institute of Technology, 500 10th Street, Atlanta, Georgia 30332, United States

[‡]National Renewable Energy Laboratory, BioEnergy Science Center, Golden, Colorado 80401, United States

Supporting Information

ABSTRACT: The average spatial dimensions between major biopolymers within the plant cell wall can be resolved using a solid-state NMR technique referred to as a ^{13}C cross-polarization (CP) SELDOM (*sel*ectively by *d*estruction *o*f *m*agnetization) with a mixing time delay for spin diffusion. Selective excitation of specific aromatic lignin carbons indicates that lignin is in close proximity to hemicellulose followed by amorphous and finally crystalline cellulose. ^{13}C spin diffusion time constants (T_{SD}) were extracted using a two-site spin diffusion theory developed for ^{13}C nuclei under magic angle spinning (MAS) conditions. These time constants were then used to calculate an average lower-limit spin diffusion length between chemical groups within the plant cell wall. The results on untreated ^{13}C enriched corn stover stem reveal that the lignin carbons are, on average, located at distances ~0.7−2.0 nm from the carbons in hemicellulose and cellulose, whereas the pretreated material had larger separations.

KEYWORDS: *^{13}C CP, SELDOM, spin diffusion, plant cell wall, corn stover*

INTRODUCTION

The plant secondary cell wall, which accounts for the majority of carbohydrates found in biomass, is a critical evolutionary adaptation, providing structural support and protection and facilitating the transport of water and nutrients. The highly functional nature of the plant cell wall directly correlates with the unique chemical and physical properties that it exhibits. These properties have been, in part, attributed to the heterogeneous, multicomponent ultrastructure of the plant cell wall.[1,2] The structure of the plant cell wall is believed to occur as a complex microstructural system composed of a lignin and hemicellulose matrix encapsulating and supporting cellulose fibrils packed into bundles.[2] The very properties that make the cell wall so useful in nature as a structural element make it difficult and expensive to biologically deconstruct.[3] Therefore, understanding the cell wall ultrastructure and its relationship to recalcitrance, the ability of the plant cell wall to resist enzymatic deconstruction, is vital for improving current biomass processing and conversion technologies for biofuel production.[3,4]

Cellulose, as shown in Figure 1, is the most abundant terrestrial source of carbon and a polysaccharide consisting of a linear chain of $\beta(1\rightarrow4)$-linked D-glucose units packed in both crystalline and amorphous morphologies in the cell wall.[1,2] The ^{13}C nuclear magnetic resonance (NMR) spectrum of cellulose is dominated by *O*-alkyl-associated carbon resonances at various chemical shifts between 105 and 65 ppm.[1] Corn stover has been considered a principal feedstock for the production of bioethanol and a variety of biomass-derived bioproducts;[5] however, corn stover was primarily chosen as a substrate in this study because its ^{13}C-enriched version is commercially available.

Along with cellulose in almost all plant cell walls including corn stover is hemicellulose. Hemicellulose is a broad class of biopolymers, consisting of several branched, heteropolymers, such as arabinoxylans, composed of both 5- and 6-carbon sugars (see Figure 1).[2,6] Hemicellulose not only generates *O*-alkyl-associated carbon NMR resonances (105−65 ppm) but also signals related to acetyl functionality with carboxylic and methyl carbons (at ~174 and 21 ppm).[7] The last major biopolymer shown in Figure 1 is lignin. Lignin is a complex, racemic, cross-linked, and highly heterogeneous aromatic macromolecule based on hydroxycinnamyl monomers with various degrees of methoxylation.[2]

Corn stover lignin is a *p*-hydroxyphenyl (H), guaiacyl (G), syringyl (S) lignin (see Figure 1), generally accounting for 20−30% of the biomass dry weight and proportions of the acetyl group content.[5] The NMR spectrum of lignin consists, in part, of aliphatic (~83−61 ppm), methoxy (~55 ppm), and substituted/unsubstituted aromatic carbons (~155−106 ppm).[8] Thioacidolysis analysis of mature maize stalks indicates the proportions of H, G, and S units in a representative sample of corn stover lignin to be about 4, 35, and 61%, respectively.[5] Other research has also shown corn stover to contain significant proportions of hydroxycinnamic acids such as ferulic acids, which have been shown to serve as bridges between lignin and polysaccharides bonding via ether and ester linkages, called lignin−carbohydrate complexes.[5] Lignin content, monolignol distribution, and lignin−carbohydrate complexes have all been cited as potential factors in biomass recalcitrance.[9]

No methods exist to isolate or separate cell wall components while keeping their native 3D ultrastructure fully intact.[10] Nondestructive methods, such as infrared-red (IR) and Raman

Received: November 28, 2011
Revised: January 8, 2012
Accepted: January 12, 2012
Published: February 1, 2012

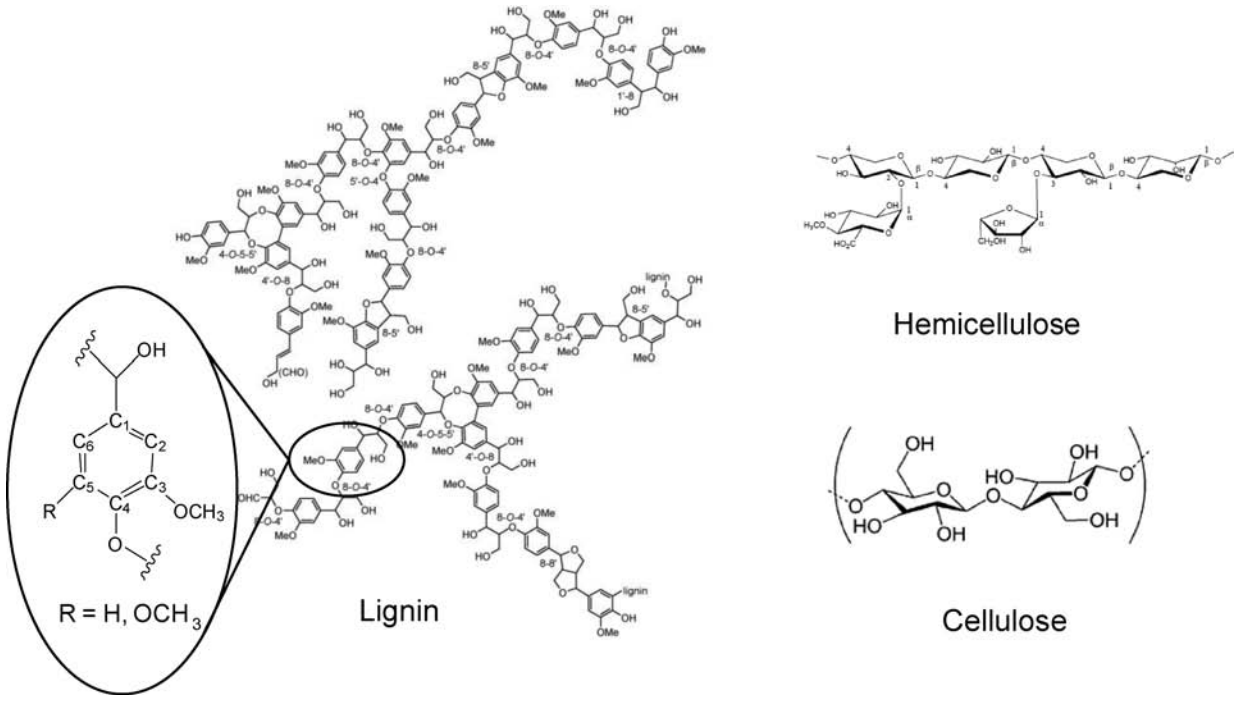

Figure 1. Major biopolymer in the plant cell wall where the lignin structure represents characteristic subunits in corn stover lignin (images taken from ref 2b) and the hemicellulose represents xylan, the main hemicellulose macromolecule. The three main monolignol units are defined as follows: *p*-hydroxyphenyl (H) units with no methoxy groups, syringyl (S) units with methoxy groups at the C_3 and C_5 positions, and guaiacyl (G) units with a methoxy group at the C_3 position.[2a]

spectroscopy, along with X-ray diffraction (XRD) and electron diffraction/microscopic methodologies, have been used to elucidate the ultrastructure of plant cell walls; however, none of these techniques alone can fully characterize the plant cell wall architecture.[1,10] Solid-state NMR spin diffusion experiments are particularly useful tools for the determination of inter- and intramacromolecular distances,[11] used typically in traditional polymer/additive systems,[12] semicrystalline polymers,[13,14] polymer blends,[15−18] block copolymers,[19] and, more recently, crystallized proteins.[20,21] Along with NMR's ability to clearly resolve various chemical and ultrastructural features in the cell wall, these types of spin diffusion experiments should be ideal for determining the spatial distribution of cell wall components.

For example, Masuda and Horii et al. conducted ^{13}C and ^{1}H spin diffusion measurements to investigate the spatial distribution of amorphous and crystalline C_4 carbons in bacterial cellulose.[22] By employing a selective inversion DANTE (*d*elays *a*lternating with *n*utation for *t*ailored *e*xcitation) π pulse sequence and ^{13}C spin diffusion on $^{13}C_4$-enriched bacterial cellulose, they found that amorphous C_4 carbons are more than likely located at distances less than about 1 nm from the crystalline C_4 carbons.[22] More interestingly, they determined that amorphous C_4 carbons are not localized to the microfibril surface[22] but are instead distributed throughout the whole volume of the cellulose, which disagrees with several cellulose microfibril models.[23−30]

The nature of biopolymer chain organization and cell wall ultrastructure can be very critical in understanding, improving and reducing the cost of enzymatic hydrolysis.[31,32] Utilizing ^{13}C proton driven spin diffusion experiments qualitatively, one would expect to observe relative distances between cell wall components based on relative spin diffusion times; moreover, it should also be possible to quantitatively determine the corresponding spin diffusion length scales. In an effort to demonstrate the viability and usefulness of these types of experiments, particularly to plant cell wall and biofuel research, ^{13}C CP selective excitation spin diffusion measurements have been conducted on ^{13}C-enriched corn stover stem material to obtain information about the relative spatial dimensions between cell wall components.

A typical step to reduce the inherent recalcitrance within the plant cell wall for enzymatic deconstruction of cellulose to glucose is thermochemical pretreatment.[33−35] A common and well-studied prehydrolysis method is dilute acid pretreatment, which reportedly removes hemicellulose through acid hydrolysis, disrupts the lignin structure, and ultimately enhances deconstruction of cellulose.[33−35] A combination of optimized pH, temperature, and pressure is utilized to minimize lignin- and carbohydrate-degradation product formation, which can cause inhibitory effects on enzymatic activity while maximizing swelling and solublization of hemicellulose.[36−38] The hydrothermal and acidic conditions used during pretreatment not only could possibly impact chemical structures in cell wall biopolymers but also affect the three-dimensional microstructure of the cell wall. Specifically, Esteghlalian et al. found corn stover pretreated at 180 °C in 0.6% H_2SO_4 for 5 min generated a substrate that had 88% of the xylan removed,[39] whereas Donohoe et al. reported that lignin droplets were formed in sizes ranging from 5 nm to 10 mm in diameter as a result of lignin coalescence, migration, and cell wall extrusion during dilute acid pretreatment of corn stover, visualized through scanning electron microscopy.[40] The resulting lignin droplet size was found to depend significantly on process severity.[40] In this study, we utilized similar dilute acid pretreatment conditions to induce changes in cell wall ultrastructure relevant to reduced recalcitrance.

NMR Background. Very few solid-state NMR experiments rely on selective pulses. Selective pulse excitation for static samples can be relatively straightforward; however, under magic angle spinning (MAS) conditions, selective excitation can be considerably more complex and difficult to execute.[41] On the basis of work done with high-resolution liquid state spectroscopy, selective pulse experiments have been shown to be quite informative and are typically used for either spectral simplification or the preparation of an initial nonequilibrium state for experiments like spin diffusion.[41] In general, selective excitation is achieved by the application of either a "soft" pulse, a weak radio frequency field of the proper frequency, or by a DANTE sequence consisting of a train of short and intense 180° radio frequency pulses for selective resonance inversion.[41,42] There are only a few examples in the literature where DANTE selective pulses have been utilized on biomass like substrates, including $^{13}C_4$-enriched bacterial cellulose[22] and coal structures[43] for spin diffusion experiments. In 1988, Canet et al. described a different method for selective excitation for MAS experiments, which takes advantage of the short T_2 times associated with ^{1}H coupled ^{13}C nuclei in the solid state, referred to as SELDOM (*sel*ectivity by *d*estruction *o*f *m*agnetization).[42] A DANTE sequence selects the resonances to remove by selective inversion or saturation, whereas SELDOM selects the resonance to retain; because of this, we chose to use the SELDOM sequence.

Selective Excitation Method by SELDOM. Figure 2 shows the pulse sequence used for the ^{13}C selective excitation cross-

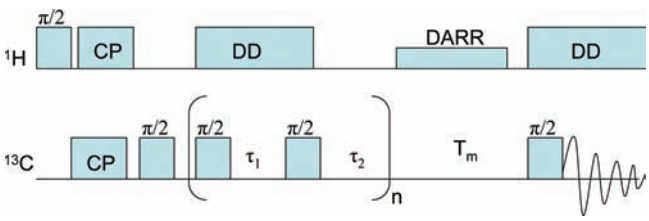

Figure 2. Schematic illustrating the ^{13}C SELDOM spin diffusion NMR (based on a sequence from ref 42). $\pi/2$ = 90° pulse; CP = cross-polarization; DD = decoupling; DARR = dipolar assisted rotational resonance, broadband recoupling; and T_m = mixing time.

polarization and spin diffusion measurements, first described by Canet et al.[42] The sequence begins as a normal cross-polarization experiment; however, after magnetization transfers to all of the carbons in the system, a carbon 90° pulse is used to store magnetization back in the *z*-direction. Directly following this, two hard carbon 90° pulses at the chosen resonance frequency are generated to retrieve and restore carbon magnetization. These pulses are separated by a short dephasing delay (denoted as τ_1) during which ^{1}H decoupling is maintained. Following the carbon restore pulse, there is an additional rotor synchronized delay (denoted as τ_2 = *i*·rotor period) during which ^{1}H decoupling is off. During the first τ_1 delay, decoupling allows magnetization to evolve under the influence of chemical shift. Through the second τ_2 delay, coupling of spins cancels transverse components of the magnetization vector. Selective excitation is achieved by repeating the sequence of retrieve and restore carbon pulses with τ_1 and τ_2 delays, progressively reducing the transverse components of the individual magnetization vectors of spectral features located away from the carrier frequency, essentially deleting magnetization of off-resonance signals.

After the SELDOM pulse train, a mixing time delay allows for spin diffusion of stored magnetization, during which dipolar-assisted rotational resonance (DARR) recoupling is utilized. MAS averages out anisotropic nuclear spin interactions, causing the nuclear spins to behave as if they were in a liquid solution, undergoing rapid, isotropic tumbling. This can reduce the effective dipolar coupling, which causes spin diffusion and is used to extract distance information. Therefore, a properly set up DARR recoupling can reintroduce dipolar interaction via broadband recoupling, increasing the effective spin diffusion distances, which can be measured at moderate spinning speeds.[50] Afterward, a final ^{13}C 90° pulse recalls magnetization after spin diffusion.

The aim of this study is not only to demonstrate the viability and usefulness of these types of experiments to resolve the spatial dimensions of major cell wall biopolymers of intact plant material but also to present data on untreated and pretreated ^{13}C-enriched corn stover, which can be used to infer a probable 3D ultrastructural cell wall model and how that structure is altered during pretreatment. This methodology on untreated, pretreated, and genetically altered plants of a wide range of species and its resulting conclusions with respect to correlations between cell wall spatial dimensions and recalcitrance is particularly significant to future improvements in biomass bioengineering and processing as well as the rational design of superior biocatalysts.

MATERIALS AND METHODS

Feedstock. ^{13}C-enriched corn stover (*Zea mayes*) stems (0.147−0.837 mm ground, >97 atom %) were purchased from IsoLife (Wageningen, Netherlands). Extractives were subsequently removed from ground samples by placing the biomass into an extraction thimble in a Soxhlet extraction apparatus. The extraction flask was filled with 1:2 ethanol:benzene mixture (~150 mL) and then refluxed at a boiling rate, which cycled the biomass for at least 24 extractions over a 4 h period.

Chemical Analysis. The preparation and analysis of samples for carbohydrate constituents and acid-insoluble residue (Klason lignin) analysis used a two-stage acid hydrolysis protocol based on TAPPI methods T-222 om-88 with a slight modification[44] following the exact experimental conditions in cited literature.[45] The preparation and analysis of samples for whole cell wall ionic liquid 1D ^{13}C and 2D ^{1}H−^{13}C heteronuclear single quantum correlation HSQC NMR analysis used an anhydrous pyridinium chloride-d_5/DMSO-d_6 solvent mixture and Bruker Avance-500 spectrometer following the exact experimental conditions in cited literature.[46,47] On the basis of cited chemical shifts, 1D and 2D NMR assignments and subsequent methods of quantification were based on literature material; these data are provided in the Supporting Information.[48,49]

NMR Spectroscopy. The center-packed NMR samples were prepared with ground biomass added into 4 mm cylindrical ceramic MAS rotors with Teflon plugs. Solid-state NMR measurements were carried out on a Bruker Avance-400 spectrometer operating at frequencies of 399.84 MHz for ^{1}H and 100.55 MHz for ^{13}C NMR in a Bruker double-resonance MAS probehead at spinning speeds of 10.1 kHz. ^{13}C CP/MAS and SELDOM spin diffusion experiments utilized a 5 μs (90°) ^{1}H and ^{13}C pulse, 2.5 ms 50 kHz HH-contact pulse, 50 kHz SPINAL-64 heteronuclear decoupling, 4 s recycle delay, 250 ppm sweep width, and 8−16 K scans. Continuous wave ^{1}H DARR recoupling utilized a rotary resonance power level of 10.1 kHz and mixing times between 0.09 and 4950 ms. Baseline-corrected spectra were processed with 75 Hz exponential line broadening.

RESULTS AND DISCUSSION

As part of this study, we also investigated the use of 2D ^{13}C−^{13}C proton-driven spin diffusion (PDSD) experiments,

similar to those utilized on site-directed ^{13}C-enriched protein samples.[20,21] In these experiments, extraction of distance information results from cross-peak intensities, recorded and analyzed for a set of spectra over various mixing times. While initial experiments were successful, the time required to acquire enough mixing time data points suggests that the most efficient route to resolving spatial dimensions in ^{13}C-enriched plant cell walls could be employing the above ^{13}C CP SELDOM sequence with spin diffusion, which is essentially the 1D version of the 2D ^{13}C−^{13}C PDSD experiment.

Sugar profiles from HPLC-based monosaccharide anionic exchange chromatography and acid-insoluble residue content of the ^{13}C-enriched untreated and pretreated corn stover were obtained to quantitatively analyze the changes in the cell wall composition and are tabulated in Table 1. The untreated ^{13}C-enriched corn stover sample was also analyzed by whole cell wall ionic liquid 1D ^{13}C and 2D ^{1}H−^{13}C HSQC NMR analysis (see the Supporting Information). One-dimensional ^{13}C NMR determine the proportions of H, G, and S units in the untreated ^{13}C-enriched corn stover lignin to be about 12, 21, and 66%, respectively. Two-dimensional ^{1}H−^{13}C HSQC NMR clearly observed the significant presence of C_2- and C_3-acetylated xylan, *β-O*-4-aryl ether lignin linkages, and ferulate and *p*-coumarate units.

Table 1. Compositional Analysis of the ^{13}C-Enriched Corn Stover

	% glucan	% xylan	% Klason lignin
control natural abundant corn stover	30	23	26
^{13}C-enriched corn stover	38	25	20
pretreated ^{13}C-enriched corn stover	68	2	22

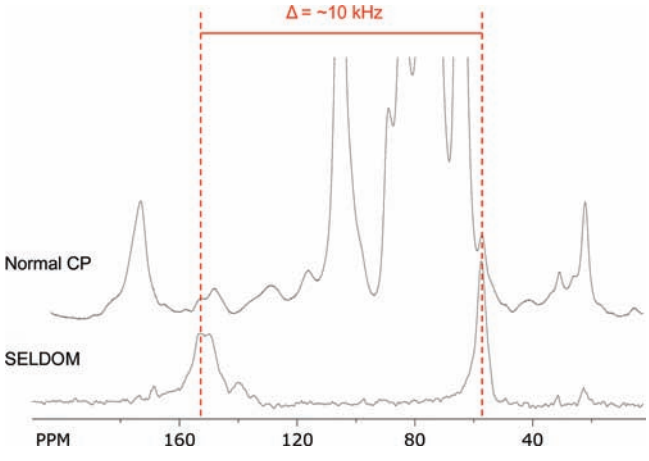

Figure 3. One-dimensional selective excitation method by SELDOM at MAS = 10.1 kHz.

Figures 3 and 4 show the normal CP spectrum of ^{13}C-enriched corn stover stem, displaying the resonances due to major chemical groups within lignin, cellulose, and hemicellulose. Throughout the remainder of this paper, various chemical moieties will be denoted by the following: A_1 carbons, which correspond to aromatic lignin carbons appearing ∼153 ppm or the $S_{3,5}$ and $G_{3,4}$ carbons; A_2 carbons corresponding to aromatic lignin carbons appearing ∼135 ppm or the $S_{1,4}$ and G_1 carbons; and A_3 carbons attributed to $S_{2,6}$ and $G_{2,5,6}$ at ∼110 ppm.[8] Other resonances of interest highlighted in Figure 4 are those for cellulose C_1, $C_{2,3,5}$, C_6, C_{4a} (amorphous C_4), and C_{4c} (crystalline C_4) at ∼105, 75, 64, 86, and 90 ppm, respectively.[1]

Hemicellulose has a ^{13}C signal that arises ∼83.9 ppm and is attributed to the C_4 carbon in the xylose monomer unit.[7] This resonance is unique to xylan chains, which are part of xylan-cellulose aggregates and typically found in combination with the hemicellulose carbonyl and methyl moieties associated with acetyl groups observed at resonances ∼174 and 21.5 ppm.[7] The resonance at 21.5 ppm also happens to be the only completely resolved hemicellulose-associated resonance. Utilizing the resonances contributing to lignin (A_1, A_2, and A_3) and hemicellulose acetyl groups and neglecting any contributions from hemicellulose to the narrow chemical shift ranges used to represent cellulose (C_{4a}, C_{4c}, and $C_{2,3,5}$), the analysis described below was utilized to generate normalized and T_1-adjusted spin diffusion attenuation curves.

The SELDOM pulse train carrier frequency was generated at the chemical shift of $S_{3,5}$ and $G_{3,4}$ carbons (∼153 ppm) in lignin. Figure 3 clearly shows how successful the SELDOM filter is at localizing magnetization in lignin-related resonances; however, signals at frequencies equaling integers of the rotor speed are not removed, as evident by the appearance of the methoxy carbon resonance at ∼55 ppm in Figure 3. In an attempt to only select aromatic carbon magnetization, rotor speeds in the excess of 16−20 kHz were tried; however, inefficient spin diffusion due to reduced dipolar interaction was observed. A better compromise seemed to be to tune the number of SELDOM pulse trains, τ_1, τ_2, and rotor speed to only select carbons only on lignin. This was done also while maximizing the selective nature of the SELDOM and the corresponding signal intensity generated. Optimum conditions were determined to be at a SELDOM pulse train carrier frequency of 153 ppm, spinning speed of 10.1 kHz, τ_1 = 99 μs, τ_2 = 594 μs, and 36 SELDOM pulse train cycles.

On the basis of signal-to-noise calculations of the methoxy peak from the normal CP and chemical shift filtered spectra, the SELDOM filter only causes ∼35% signal loss in the selected areas, while effectively removing magnetization from all of the other carbons. The implication of this in a system in which the selected carbon resonances only correspond to a small fraction of the overall carbon (∼3 of 10 carbons in a monolignol unit in a system with ∼10−15% lignin) is a resulting loss of the total magnetization by spectral integration of ∼95%. This essentially reduces the amount of initial nonequilibrium magnetization such that upon equilibration the spectrum has a low S/N requiring a large number of scans; however, in systems with less diffusive chemical shift distributions and a high proportion carbon in the selected region, this technique can be particularly simplistic and quick to conduct.

^{13}C Spin Diffusion Length Scale Estimations. Once the SELDOM sequence is applied and magnetization localized on the lignin-associated $S_{3,5}$, $G_{3,4}$, and methoxy carbons, the actual mechanism of signal attenuation during the spin diffusion experiment is fairly complex. This is mainly because magnetization is not just transferring between major cell wall components but is actually moving from multiple chemical moieties distributed heterogeneously among the lignin chains to their nearest neighbors. However, as an initial approximation, these experiments can be analyzed in terms of a three- or two-site model given in Figure 5. In these models, magnetization is assumed to fully equilibrate in the lignin and then move to the other cell wall components.

dx.doi.org/10.1021/jf204853b | J. Agric. Food Chem. 2012, 60, 1419−1427

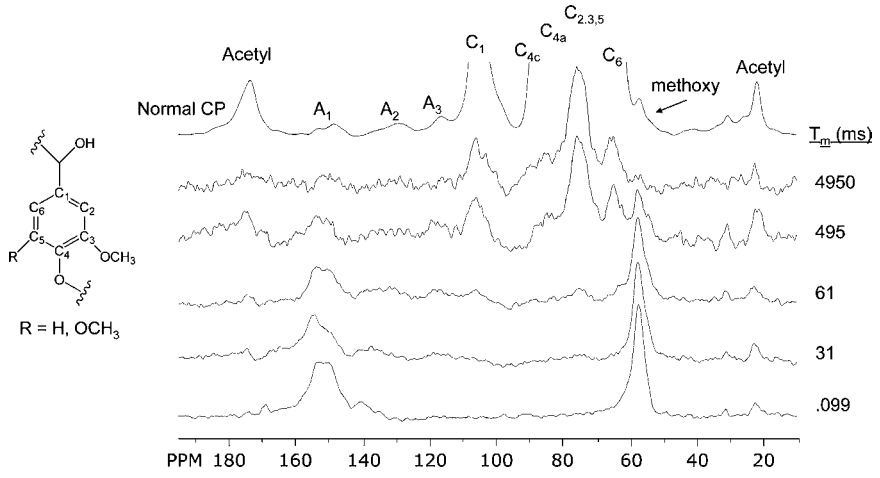

Figure 4. Normal CP (top) and ^{13}C selective excitation and spin diffusion experiments of ^{13}C-enriched corn stover stem.

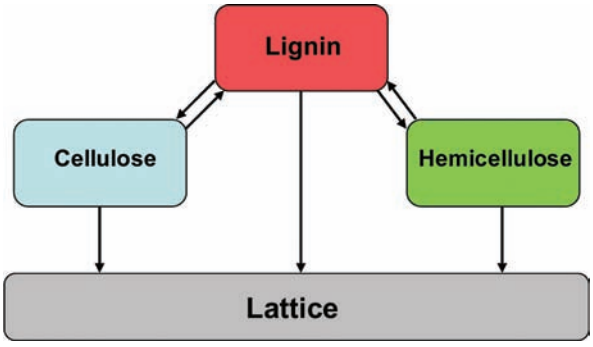

Figure 5. Three-site model used for evaluation of the ^{13}C spin diffusion and ^{13}C spin−lattice relaxation phenomena occurring in the plant cell wall.

Figure 5 visually depicts the intrinsic longitudinal relaxation occurring in the lignin, cellulose, and hemicellulose cell wall fractions with downward vertical arrows and the cross-relaxation equilibrium phenomena, represented by diagonal arrows. Although this three-site model more describes the actual system, for mathematical model simplification, two two-site exchange models were used to extract spin diffusion length scales and spatial dimensions. This model assumes transfer occurs between lignin and hemicellulose, while another assumes transfer between lignin and cellulose.

During the spin diffusion mixing time, the change in magnetization of a given ^{13}C nucleus i is related to both ^{13}C spin diffusion and ^{13}C spin−lattice relaxation (T_1), which is given by:

$$\frac{dM_i}{dt} = -\frac{M_i - M_i^{eq}}{T_{1C,i}} - \frac{M_i - M_i^{eq}}{T_{SD}} + \frac{M_j - M_j^{eq}}{T_{SD}} \quad (1)$$

where M_i^{eq} and M_j^{eq} are the equilibrium magnetizations of the nuclei i and j, respectively, and T_{SD} and $T_{1C,i}$ are the time constants for the ^{13}C spin diffusion and the ^{13}C spin−lattice relaxation for the nucleus i, respectively.[22] This equation describes a two-site spin diffusion model. The solution and further simplification of eq 1 is

$$\frac{M(t)}{M(0)} = A \exp\left(-\frac{2t}{T_{SD}}\right)\exp\left(-\frac{t}{T_{1C,i}}\right) + B \quad (2)$$

In an effort to account for ^{13}C spin−lattice relaxations, the sequence in Figure 1 was used with no SELDOM selection. This experiment is essentially measuring the T_1 attenuation occurring during the mixing time. By dividing the relative intensity of the ^{13}C SELDOM spin diffusion experiments by the relative intensity resulting from those experiments, eq 2 can be reduced to

$$\frac{\frac{M(t)}{M(0)}}{\frac{M_{T_{1C,i}}(t)}{M_{T_{1C,i}}(0)}} = A \exp\left(-\frac{2t}{T_{SD}}\right) + B \quad (3)$$

As denoted by Masuda and Horii et al., the average ^{13}C spin diffusion rate, $\overline{Wij}$, between spin i and j under the MAS condition is given by:

$$\frac{1}{T_{SD}} \approx \overline{W_{ij}} = \frac{1}{2}\pi\,\overline{\omega_{ij}^2}\overline{F_{if}(0)} \quad (4)$$

where ω_{ij} is the dipolar coupling frequency and $F(0)$ is the probability for single quantum spin transitions for spins i and j.[22] The ω_{ij} term integrates distance information,

$$\overline{\omega_{ij}^2} = \overline{\left[\frac{1}{2}\gamma_c^2\hbar r_{ij}^{-3}(1 - 3\cos^2\theta_{ij})\right]^2} \quad (5)$$

therefore, T_{SD} and spin diffusion length scales as,

$$\frac{1}{T_{SD}} \approx \frac{K}{r^6} \quad (6)$$

where K is a spin diffusion coefficient.[22]

Figure 4 shows the normal CP spectrum of ^{13}C-enriched corn stover stem in a stacked plot along with SELDOM spin diffusion spectra of increasing T_m or mixing time. At the shortest mixing time, the spectra show the SELDOM filter to be effective at isolating magnetization in the methoxy and A_1 ($S_{3,5}$ and $G_{3,4}$) carbons. As the mixing time increases, magnetization is transferred to other groups in the lignin and then to the carbohydrate carbons, presumably first to hemicellulose and then to cellulose based on the rapid appearance of the acetyl-related methyl peak at ~21 ppm. The mathematical treatment described above is based on a simple 1D spin diffusion theory developed for ^{13}C nuclei under MAS condition.[22] Determining the ^{13}C spin diffusion length

dx.doi.org/10.1021/jf204853b | J. Agric. Food Chem. 2012, 60, 1419−1427

requires previous knowledge of the spin diffusion coefficient. Unfortunately, spin diffusion coefficients are difficult to measure or estimate by nuclear spin density,[51] so the data were analyzed utilizing two strategies: (1) determining the spin diffusion rate based on known inter-ring distances between lignin aromatic carbon positions and (2) using a spin diffusion rate cited in the literature determined for ^{13}C-enriched bacterial cellulose.

A simple exponential fit (as described in eq 3) was applied to ^{13}C spin diffusion attenuation curves to determine the characteristic ^{13}C spin diffusion time constant (T_{SD}) of each resonance of interest. Figure 6 shows normalized and T_1-adjusted spin diffusion peak intensities as a function of mixing time. As evident in Figure 6a, which contains results from aromatic resonances, the spin diffusion occurs in two stages within the lignin, inter- and intramolecular equilibration. Because of this, the data were not normalized by the intensity at time = 0 but rather the maximum value integral, and eq 3 was fit separately to the first three and last four data points for the aromatic lignin signals. Additionally, eq 3 was applied to the full spin diffusion attenuation curve of the hemicellulose and cellulose signals, as shown in Figure 6b.

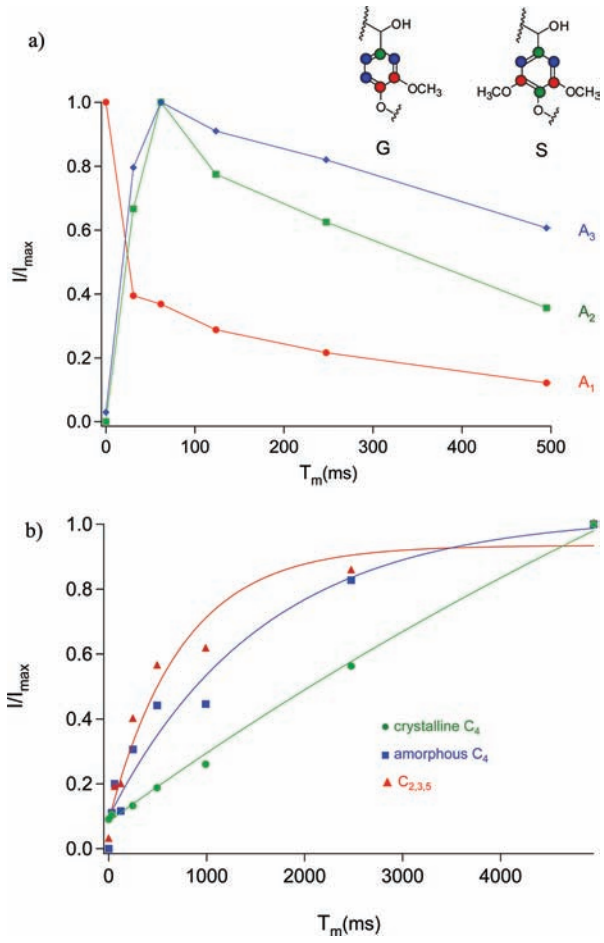

Figure 6. Plots of normalized and T_1-adjusted peak intensities of the (a) A_1 (red), A_2 (green), and A (blue) resonance lines shown in Figure 2 against T_m values and (b) cellulose $C_{2,3,5}$ (red), C_{4a} (blue), and C_{4c} (green). The solid lines in the right plot only serve to follow trends and in the left plot are obtained by the least-squares method based on eq 3.

As mentioned before, determining K can be difficult; therefore, we took two approaches, using K as determined by an average distance of ~1.9 Å between A_1 and A_2 carbons (K = 5.315 × 10^{-61} m^6/ms) and using a K determined by Masuda and Horii et al. for ^{13}C-enriched crystalline bacterial cellulose (K = 2.75 × 10^{-57} m^6/ms) estimated by its nuclear density.[22] The spin diffusion times and calculated spin diffusion lengths resulting from eq 6 are compiled in Table 2. Much of this analysis was based on work by Masuda and Horii et al. and seems to agree at least within an order of magnitude with spin diffusion lengths with ^{13}C-enriched crystalline bacterial cellulose.

Table 2. Time Constants (T_{SD}) for the ^{13}C Spin Diffusion and the Diffusion Lengths (r) for Different Carbon Species

resonance assignment	T_{SD} (ms)	r (Å)[a]	r (Å)[b]
cellulose-C_6	702	2.7	11.2
cellulose-$C_{2,3,5}$	1481	3.0	12.6
cellulose-C_{4c}	22472	4.8	19.9
cellulose-C_{4a}	313	2.3	9.8
cellulose-C_1	2020	3.2	13.3
acetyl-carboxyl	250	2.3	9.4
acetyl-methyl	78	1.9	7.7
A3	47	1.7	7.1
A2	88	1.9	7.9

[a] K = 5.315 × 10^{-61} m^6/ms. [b] K = 2.75 × 10^{-57} m^6/ms.[19]

The shortest spin diffusion length (~0.77 nm) corresponds to the spin diffusion from lignin to a neighboring acetylated hemicellulose residue; as a reference, consider that the size of one cellobiose residue is ~0.5 nm in radius. Therefore, lignin and hemicellulose are on average less than two cellobiose residues from one another. The calculated spin diffusion length from lignin to an acetyl group is very similar whether determined with the methyl or carbonyl carbon, seemingly supporting the validity of the analysis. The next spin diffusion length, in increasing order, seems to be closely associated with the spin diffusion from lignin to a neighboring amorphous C_4 carbon on a glucose residue (~0.98 nm). The other calculated spin diffusion lengths range from ~1.12−1.33 nm for the C_1, C_2, C_3, C_5, and C_6 carbons. Lastly, the longest diffusion length (~1.99 nm) is related to the spin diffusion from lignin to a neighboring crystalline C_4 carbon on a glucose residue. Interestingly, the other carbon cellulose sites appear to be a weighted average of the distances calculated for C_{4a} and C_{4c}. The results also seem to suggest that lignin is in close contact with both hemicellulose and cellulose, especially considering that all calculated lengths are much smaller than the size of a cellulose microfibril (4−6 nm). The spin diffusion lengths for the C_4 carbon suggest that amorphous cellulose is indeed closer to lignin than crystalline cellulose, generating a core−shell interpretation, with the amorphous shell being ~1 nm thick and in the most contact with lignin.

In an effort to demonstrate the usefulness of this technique on a range of biomass samples and especially in studies intended to evaluate changes in the spatial relationships between cell wall biopolymers, Figure 7 shows the normal CP spectrum of ^{13}C-enriched corn stover stem, which was pretreated at 180 °C in 1.2% H_2SO_4 for 5 min in a stacked plot along with SELDOM spin diffusion spectra of increasing T_m. Again, the spectra corresponding to the shortest mixing time clearly indicate the SELDOM filter was effective at isolating

dx.doi.org/10.1021/jf204853b | J. Agric. Food Chem. 2012, 60, 1419−1427

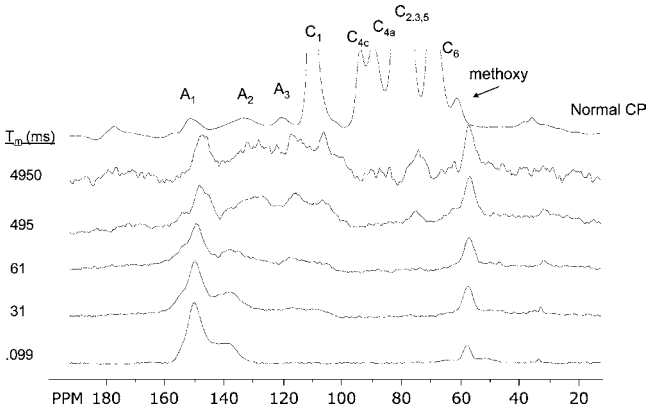

Figure 7. Normal CP (top) and ^{13}C selective excitation and spin diffusion experiments of pretreated ^{13}C-enriched corn stover stem (180 °C/5 min/1.2% H_2SO_4).

magnetization in the methoxy, $S_{3,5}$, and $G_{3,4}$ carbons. Unlike Figure 5, Figure 7 indicates significant magnetization transfer between the lignin and the cellulose does not occur even at the longest mixing time. This suggests that either lignin has aggregated beyond the length scale of which magnetization can transfer before nuclear spin−lattice relaxation begins to dominate and/or the extraction of hemicellulose by acid hydrolysis removed the major physical connection between lignin and cellulose. Using the spin diffusion coefficient calculated by Masuda and Horii et al., a mixing time delay of 4950 ms corresponds to a spin diffusion length of ∼2 nm. On the basis of this, longer mixing time delays should be used on the pretreated samples; however, although the ^{13}C T_1 times for amorphous and crystalline cellulose may be ∼15 and 30 s,[52] respectively, the T_1 times of chemical groups on lignin have been cited as between 0.7 and 2.5 s,[53] which corresponds to ∼85−99% lost in signal intensity. This fact combined with the low lignin content in corn stover (10−15%) made ∼5 s the longest mixing time in which sufficient signal-to-noise at 16 K scans was obtained, even for a highly ^{13}C-enriched sample.

Figure 3 clearly shows the SELDOM sequence-localized magnetization within chemical moieties on the lignin, while Figure 5 displays that magnetization transfer does occur to other carbon sites as a function of increasing mixing time. All calculated spin diffusion length scales on the untreated sample seem to be within 2 nm, suggesting that the plant cell wall structure is intimately blended. In an ideal experiment, two spin diffusion coefficients would be determined, since the spin diffusion rates are mainly a function of nuclear spin density and residual dipolar interactions, and will change inter- and intramolecularly. Therefore, the spatial dimensions determined more than likely represent lower limits, as nuclear spin density and dipolar interactions vary nonuniformly throughout the cell wall; moreover, the spin diffusion rate may further change with the possibility of variable chain dynamics, such as freely rotating methyl groups on methoxy functionality.

In conclusion, the results, on average, seem to suggest that lignin is in close contact with both hemicellulose and cellulose, indicating methyl carbons on acetyl groups followed by carbonyl carbons on acetyl groups line the interface between hemicellulose and lignin. The C_4 results show the amorphous cellulose to be closer to lignin than crystalline cellulose, suggesting a core−shell model, with the amorphous shell being ∼1 nm thick. The other carbon cellulose sites appear to be an average of the distances calculated for C_{4a} and C_{4c}, further supporting the validity of the results. The ^{13}C CP SELDOM spin diffusion experiments on the pretreated sample did not indicate that significant magnetization transfer between the lignin and the cellulose occurs even at the longest mixing time. This suggests that either lignin has aggregated beyond the length scale of which magnetization can transfer before nuclear spin−lattice relaxation begins to dominate and/or the extraction of hemicellulose by acid hydrolysis removed the major physical connection between lignin and cellulose such that the system is no longer intimately mixed. This seems to confirm the previous claim that hemicellulose, which is removed in the pretreated sample by acid hydrolysis, lies at the interface between lignin and amorphous cellulose. We believe this is evidence of one of the major mechanisms of pretreatment, the removal of the hemicellulose layer disrupts the hemicellulose−lignin matrix, leaving behind voids in the secondary cell wall and increasing cellulose accessibility. In the future, a particularly interesting experiment could involve genetically altered substrates that display vastly altered recalcitrance to untreated samples, probing the spatial relationships of cell wall biopolymer as a function of genetic manipulation and how that may be related to biomass recalcitrance.

■ ASSOCIATED CONTENT

Ⓢ Supporting Information

^{13}C NMR spectral data of ^{13}C-enriched corn stover dissolved in anhydrous pyridinium chloride-d_5/DMSO-d_6 solvent mixture. This material is available free of charge via the Internet at http://pubs.acs.org.

■ AUTHOR INFORMATION

Corresponding Author

*Tel: 1-404-894-970. Fax: 1-404-894-4778. E-mail: Art.Ragauskas@chemistry.gatech.edu.

Funding

This work was supported and performed as part of the BioEnergy Science Center. The BioEnergy Science Center is a U.S. Department of Energy Bioenergy Research Center supported by the Office of Biological and Environmental Research in the DOE Office of Science. ORNL is managed by UT-Battelle, LLC, under contract DE-AC05-00OR22725 for the U.S. Department of Energy.

■ REFERENCES

(1) Atalla, R. H. Cellulose. In *Comprehensive Natural Products Chemistry*; Barton, D., Nakanishi, K., Meth-Cohn, O., Eds.; Elsevier: Amsterdam, Netherlands, 1999; Vol. 3.

(2) (a) Fengel, F.; Wegener, G. *Wood: Chemistry, Ultrastructure, Reaction*; Walter de Gruyter: New York, 1984. (b) https://public.ornl.gov/site/gallery/originals/Contemporary_View_of_L.jpg.

(3) Pu, Y.; Zhang, D.; Singh, P. M.; Ragauskas, A. J. The new forestry biofuels sector. *Biofuels, Bioprod. Biorefin.* **2008**, *2*, 58−73.

(4) Ragauskas, A. J.; Williams, C. K.; Davison, B. H.; Britovsek, G.; et al. The Path Forward for Biofuels and Biomaterials. *Science* **2006**, *311*, 484−489.

(5) Buranov, A.; Mazza, G. Lignin in straw of herbaceous crops. *Ind. Crops Prod.* **2008**, *28*, 237−259.

(6) Sada, B C. Hemicellulose bioconversion. *J. Ind. Microbiol. Biotechnol.* **2003**, *30*, 279−291.

(7) Teleman, W.; Larsson, P. T.; Iversen, T. On the accessibility and structure of xylan in birch kraft pulp. *Cellulose* **2001**, *8*, 209−215.

(8) Hatcher, P. G. Chemical structural studies of natural lignin by dipolar dephasing solid-state ^{13}C nuclear magnetic resonance. *Org. Geochem.* **1987**, *11*, 31−39.
(9) Chundawat, S.; Donohoe, B.; Sousa, L.; Elder, T.; Agarwal, U.; et al. Multi-scale visualization and characterization of lignocellulosic plant cell wall deconstruction during thermochemical pretreatment. *Energy Environ. Sci.* **2001**, *4*, 973−984.
(10) Jung, H. G.; Terashima, N.; Fukushima, K.; He, L. F.; Takabe, K. Comprehensive Model of the Lignified Plant Cell Wall. In *Forage Cell Wall Structure and Digestibility*; Ralph, J., Ed.; American Society of Agronomy, Inc.: Madsion, WI, 1993.
(11) Schmidt-Rohr, K.; Spiess, H. *Multidimensional Solid-State NMR and Polymers*; Academic Press Inc.: San Deigo, CA, 1994.
(12) Quijada-Garrido, I.; Wilhelm, M.; Spiess, H. W.; Barrales-Rienda, J. M. Solid State NMR Studies of Structure and Dynamics of Erucamide/isotactic-Poly(propylene) Blends. *Macromol. Chem. Phys.* **1998**, *199*, 985.
(13) Leisen, J.; Beckham, H. W.; Sharaf, M. A. Evolution of Crystallinity, Chain Mobility, and Crystallite Size during Polymer Crystallization. *Macromolecules* **2004**, *37*, 8028−8034.
(14) Demco, D.; Johansson, A.; Tegenfeldt, J. Proton spin diffusion for spatial heterogeneity and morphology investigations of polymers. *Solid State Nucl. Magn. Reson.* **1995**, *4*, 13−38.
(15) Matsumoto, A.; Egama, Y.; Matsumoto, T.; Horii, F. Miscibility of Polyoxymethylene Blends as Revealed by High-resolution Solid-state ^{13}C-NMR Spectroscopy. *Polym. Adv. Technol.* **1997**, *8*, 250.
(16) Brus, J.; Dybal, J.; Schmidt, P.; Kratochvl, J.; Baldrian, J. Order and Mobility in Polycarbonate−Poly(ethylene oxide) Blends Studied by Solid-State NMR and Other Techniques. *Macromolecules* **2000**, *33*, 6448−6459.
(17) Schantz, S. Structure and mobility in poly(ethylene oxide)/poly (methyl methacrylate) blends investigated by ^{13}C solid-state NMR. *Macromolecules* **1997**, *30*, 1419−1425.
(18) Zhang, X.; Takegoshi, K.; Hikichi, K. Poly(vinylphenol)/poly(methyl acrylate) and poly(vinylphenol)/poly(methyl methacrylate) blends: Hydrogen bonding, miscibility, and blending effects on molecular motions as studied by carbon-13 CP/MAS NMR. *Macromolecules* **1991**, *24*, 5756−5762.
(19) Cai, W. Z.; Schmidt-Rohr, K.; Eggera, N.; Gerharz, B.; Spiess, H. W. A solid-state N.M.R. study of microphase structure and segmental dynamics of poly(styrene-*b*-methylphenylsiloxane) diblock copolymers. *Polymer* **1993**, *34*, 267−276.
(20) Manolikas, T.; Herrmann, T.; Meier, B. H. Protein Structure Determination from ^{13}C Spin-Diffusion Solid-State NMR Spectroscopy. *J. Am. Chem. Soc.* **2008**, *130*, 3959−3966.
(21) Castellani, F.; Rossum, B.; Diehl, A.; Schubert, M.; Rehbein, K.; Oschkinat, H. Structure of a protein determined by solid-state magic-angle-spinning NMR spectroscopy. *Nature* **2002**, *420*, 98−102.
(22) Masuda, K.; Adachi, M.; Hirai, A.; Yamamoto, H.; Kaji, H.; Horii, F. Solid-state ^{13}C and ^{1}H spin diffusion NMR analyses of the microfibril structure for bacterial cellulose. *Solid State Nucl. Magn. Reson.* **2003**, *23*, 198−212.
(23) Bergenstrhle, M.; Wohlert, J.; Larsson, P. T.; Mazeau, K.; Berglund, L. A. Dynamics of Cellulose−Water Interfaces: NMR Spin−Lattice Relaxation Times Calculated from Atomistic Computer Simulations. *J. Phys. Chem. B* **2008**, *112*, 2590−2595.
(24) Virtanen, T.; Maunu, S. L.; Tamminen, T.; Hortling, B.; Liitia, T. Changes in fiber ultrastructure during various kraft pulping conditions evaluated by ^{13}C CPMAS NMR spectroscopy. *Carbohydr. Polym.* **2008**, *73*, 156−163.
(25) Huex, L.; Dinand, E.; Vignon, M. R. Structural aspects in ultrathin cellulose microfibrils followed by ^{13}C CP-MAS NMR. *Carbohydr. Polym.* **1999**, *40*, 115−124.
(26) Hult, E. L.; Larsson, T.; Iverson, T. A comparative CP/MAS ^{13}C-NMR study of cellulose structure in spruce wood and kraft pulp. *Cellulose* **2000**, *7*, 35−55.
(27) Hult, E. L.; Larsson, T.; Iverson, T. Cellulose fibril aggregation—An inherent property of kraft pulps. *Polymer* **2001**, *42*, 3309−3314.
(28) Hult, E. L.; Larsson, T.; Iverson, T. A Comparative CP/MAS ^{13}C-NMR Study of the Supermolecular Structure of Polysaccharides in Sulphite and Kraft Pulps. *Holzforschung* **2002**, *56*, 179−184.
(29) Hult, E. L.; Liitia, T.; Maunu, S. L.; Hortling, B.; Iverson, T. A CP/MAS 13C-NMR study of cellulose structure on the surface of refined kraft pulp fibers. *Carbohydr. Polym.* **2002**, *49*, 231−234.
(30) Hult, E. L.; Iverson, T.; Sugiyama, J. Characterization of the supermolecular structure of cellulose in wood pulp fibres. *Cellulose* **2003**, *10*, 103−110.
(31) Lee, S.; Kim, I. Structural Properties of Cellulose and Cellulase Reaction Mechanism. *Biotechnol. Bioeng.* **1983**, *XXV*, 3−51.
(32) Himmel, M. E.; Ding, S.; Johnson, D. K.; Adney, W. S.; et al. Biomass Recalcitrance: Engineering Plants and Enzymes for Biofuels Production. *Science* **2007**, *314*, 804−807.
(33) Wyman, C. E.; Dale, B. E.; Elander, B. T.; Holtzapple, M.; Ladisch, M. R.; Lee, Y. Y. Coordinated development of leading biomass pretreatment technologies. *Biores. Technol.* **2005**, *96*, 1959−1966.
(34) Mosier, N.; Wyman, C.; Dale, B.; Elander, R.; Lee, Y.; Holtzapple, M.; Ladisch, M. Features of promising technologies for pretreatment of lignocellulosic biomass. *Bioresour. Technol.* **2005**, *96*, 673−686.
(35) Kumar, P.; Barrett, D.; Delwiche, M.; Stroeve, P. Methods for Pretreatment of Lignocellulosic Biomass for Efficient Hydrolysis and Biofuel Production. *Ind. Eng. Chem. Res.* **2009**, *48*, 3713−3729.
(36) Soderstrom, J.; Pilcher, L.; Galbe, M.; Zacchi, G. Two-step steam pretreatment of softwood by dilute H_2SO_4 impregnation for ethanol production. *Biomass Bioenergy* **2003**, *24*, 475−486.
(37) Soderstrom, J.; Galbe, M.; Zacchi, G. Separate versus Simultaneous Saccharification and Fermentation of Two-Step Steam Pretreated Softwood for Ethanol Production. *J. Wood Chem. Technol.* **2005**, *25*, 187−202.
(38) Schell, D. J.; Farmer, J.; Newman, M.; McMillan, J. D. Dilute−Sulfuric Acid Pretreatment of Corn Stover in Pilot-Scale Reactor. *Appl. Biochem. Biotechnol.* **2003**, *105*−*108*, 69−85.
(39) Esteghlalian, A.; Hashimoto, A.; Fenske, J.; Penner, M. Modeling and Optimization of the Dilute-Sulfuric-Acid Pretreatment of Corn Stover, Poplar and Switchgrass. *Bioresour. Technol.* **1997**, *59*, 126−139.
(40) Donohoe, B. S.; Decker, S. R.; Tucker, M. P.; Himmel, M. E.; Vinzant, T. B. Visualizing Lignin Coalescence and Migration Through Maize Cell Walls Following Thermochemical Pretreatment. *Biotechnol. Bioeng.* **2008**, *101*, 913−925.
(41) Caravatti, P.; Bodenhausen, G.; Ernst, R. R. Selective Pulse Experiments in High-Resolution Solid State NMR. *J. Magn. Reson.* **1983**, *55*, 88−103.
(42) Tekely, P.; Brondeau, J.; Elbayed, K.; Retournard, A.; Canet, D. A Simple Pulse Train, Using 90" Hard Pulses, for Selective Excitation in High-Resolution Solid-State NMR. *J. Magn. Reson.* **1988**, *80*, 209−216.
(43) Sethi, N. K. *Spin Diffusion and Selective Excitation NMR Techniques for Coal Structure Studies*; Amoco Oil Research Department: Naperville, IL; pp 714−720.
(44) Davis, M. A Rapid Modified Method for Compositional Carbohydrate Analysis of Lignocellulosics by High pH Anion-Exchange Chromatography with Pulsed Amperometric Detection (HPAEC/PAD). *Wood. Chem. Technol.* **1998**, *18*, 235−252.
(45) Foston, M.; Hubbell, C.; Ragauskas, A. J. Cellulose Isolation Methodology for NMR Analysis of Cellulose Ultrastructure. *Materials* **2001**, *4*, 1985−2002.
(46) Jiang, N.; Pu, Y.; Samuel, R.; Ragauskas, A. J. Perdeuterated pyridinium molten salt (ionic liquid) for direct dissolution and NMR analysis of plant cell walls. *Green Chem.* **2009**, *11*, 1762−1756.
(47) Pu, Y.; Jiang, N.; Ragauskas, A. J. Ionic Liquid as a Green Solvent for Lignin. *Wood. Chem. Technol.* **2007**, *27*, 23−33.
(48) Samuel, R.; Pu, Y.; Raman, B.; Ragauskas, A. J. Structural Characterization and Comparison of Switchgrass Ball-milled Lignin Before and After Dilute Acid Pretreatment. *Appl. Biochem. Biotechnol.* **2010**, *162*, 62−74.

(49) Hoon, K.; Rahpl, J. Solution-state 2D NMR of ball-milled plant cell wall gels in DMSO-d_6/pyridine-d_5. *Org. Biomol. Chem.* **2010**, *8*, 576−579.
(50) Takegoshi, K.; Nakamura, S.; Terao, T. $^{13}C-^{1}H$ dipolar-assisted rotational resonance in magic-angle spinning NMR. *Chem. Phys. Lett.* **2001**, *344*, 631−637.
(51) Nagapudi, K.; Leisen, J.; Beckham, H. W.; Gibson, H. W. Solid-State NMR Investigations of Poly[(acrylonitrile)-rotaxa-(60-crown-20)]. *Macromolecules* **1999**, *32*, 3025−3033.
(52) Newman, R. Estimation of the Relative Proportions of Cellulose I_a and I_b in Wood by Carbon-13 NMR Spectroscopy. *Holzforschung* **1999**, *53*, 335−340.
(53) Dria, K. J.; Sachleben, J. R.; Hatcher, P. G. Solid-State Carbon-13 Nuclear Magnetic Resonance of Humic Acids at High Magnetic Field Strengths. *J. Environ. Qual.* **2002**, *31*, 393.